2019 IEEE International Ultrasonics Symposium (IUS)
Glasgow, Scotland, October 6-9, 2019

DNN Beamforming for High Contrast Targets in the Presence of Reverberation Clutter

Adam Luchies and Brett Byram
Department of Biomedical Engineering
Vanderbilt University
Nashville, TN, USA
E-mail: adam.c.luchies@vanderbilt.edu

***Abstract*—We evaluated training deep neural network (DNN) beamformers for the task of high contrast imaging in the presence of reverberation clutter. Training data was generated using simulated hypoechoic cysts and a pseudo nonlinear method for generating reverberation clutter. Performance was compared to standard delay-and-sum (DAS) beamforming on simulated hypoechoic cysts having a different size. For a hypoechoic cyst in the presence of reverberation clutter, when the intrinsic contrast ratio (CR) was -10 dB and -20 dB, the measured CR for DAS beamforming was -9.2±0.8 dB and -14.3±0.5 dB, respectively, and the measured CR for DNNs was -10.7±1.4 dB and -20.0±1.0 dB, respectively. For a hypoechoic cyst with -20 dB intrinsic CR, the contrast-to-noise ratio (CNR) was 3.4±0.3 dB and 4.3±0.3 dB for DAS and DNN beamforming, respectively. These results show that DNN beamforming was able to extend contrast ratio dynamic range (CRDR) by about 10 dB while also improving CNR.**

Keywords—beamforming, reverberation, deep neural networks, high contrast targets

I. Introduction

B-mode ultrasound is known to misrepresent high contrast targets because true structure can be masked by strong off-axis scattering. For example, members of our group previously noted that delay-and-sum (DAS) beamforming has limited contrast ratio dynamic range (CRDR), which causes contrast to be reduced in magnitude relative to true contrast for hyperechoic and hypoechoic targets [1]. Others have also noted that many adaptive beamformers suffer from a dark region artifact that affects high contrast targets [2].

Furthermore, reverberation clutter has been identified as a major source of image degradation for B-mode ultrasound [3]. Reverberation clutter further reduces CRDR and enhances the dark region artifact [1]. Previously, members of our group developed a physics model-based beamforming method called aperture domain model image reconstruction (ADMIRE) with the goal of suppressing reverberation clutter [4]. Developing an ultrasound beamformer that is able to accurately represent the true contrast of a high contrast target in the presence of strong reverberation clutter would improve overall B-mode image quality in high contrast imaging scenarios such as the differentiation of simple and complex cysts, cardiac ultrasound, and kidney stone imaging.

Recently, there has been growing interest in using deep neural networks (DNNs) to improve ultrasound beamforming. We developed a DNN beamformer that operates on gated segments of channel data in the frequency domain for suppressing off-axis scattering [5-6]. Hyun et. al developed a DNN beamformer for smoothing speckle [7].

Previously, we studied training DNN beamformers for high contrast targets [8]. For the current work, we investigated training deep neural network (DNN) beamformers to extend CRDR in the presence of reverberation clutter. Training data was generated from high contrast targets in the presence of reverberation clutter. The neural networks were trained to map from a region of signal space that included signal of interest, strong off-axis scattering, and reverberation clutter to the corresponding signal of interest space only.

II. Methods

The DNN beamformer studied in this work consists of a set of DNNs that operate on channel data that has been transformed to the frequency domain using a short-time Fourier transform (STFT). This DNN beamformer is convolutional in nature because the networks, including their weights, are reused through depth; however, fully connected layers are used across the aperture dimension. An inverse short-time Fourier transform (ISTFT) was used to convert back to the time-domain after DNN processing. During STFT processing, a rectangular window with one pulse length was used and the window overlap was 90%. More specific details about the beamformer studied here can be found in our previous work [5-6].

For this work, we modified the training data generation method that we introduced previously for generating training data from high contrast targets in order to incorporate reverberation clutter [8]. FIELD II was used to generate anechoic cysts and anechoic backgrounds as illustrated in Fig. 1

The authors acknowledge the support of NIH R01EB020040 and by NSF award IIS-1750994..

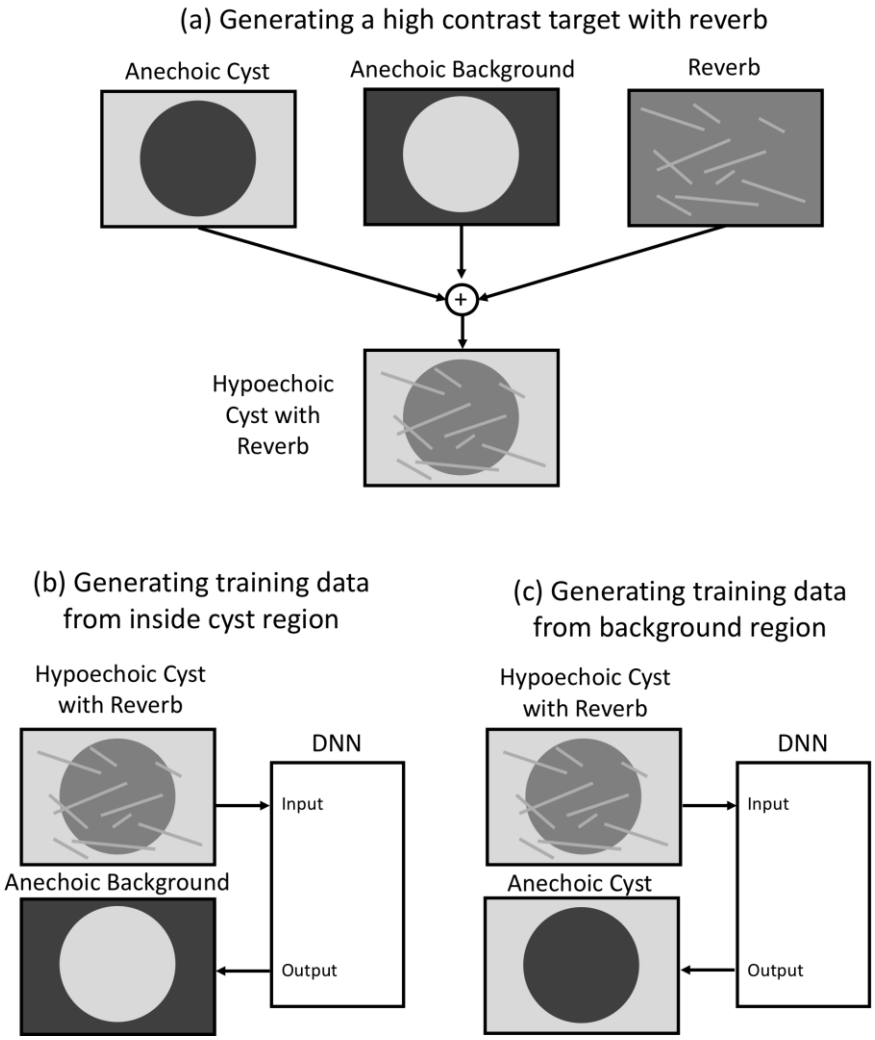

Fig. 1. (a) Method for simulating high contrast targets with reverberation clutter. Diagram for generating training data from the (b) inside of hypoechoic cysts and from the (c) background region of hypoechoic cysts.

[9]. In addition, a pseudo-nonlinear method for generating reverberation clutter that was previously developed by members of our group was used to generate reverberation clutter [10]. These channel data sets were combined as illustrated in Fig. 1 (a) in order to form hypoechoic cysts with varying contrast ratios (CR) and with a specific signal-to-clutter ratio (SCR).

Input training examples were formed from the inside of the hypoechoic cyst and also from the background region. For input examples that were created from the inside of the hypoechoic cyst with reverberation, the desired output was the paired data from the anechoic background region as illustrated in Fig. 1 (b). For input examples that were created from the background region with reverberation, the desired output was the paired data from the anechoic cyst as illustrated in Fig. 1 (c).

The set of cysts that were used for generating training data had a diameter of 1 cm. A total of 24 cysts were simulated and each cyst provided 6,328 training examples. The CR was varied from -40 dB to 0 dB in steps of 2 dB. The signal-to-clutter ratio (SCR) was 0 dB. An equal number of examples were drawn from the inside and the background regions. The total number of training examples included in the training data set was 3,189,312. All of the cysts were located at a depth of 7 cm.

The set of cysts that were used to generate examples for the test set had a diameter of 5 mm. The test set had three cysts and each cyst provided 1,392 training examples. The total number of examples in the test set was 87,696.

The simulated array was modeled after an L7-4 linear array transducer, with a scanning aperture of 65 elements on transmit and receive, 298 μm pitch, 48 μm kerf , 7 cm transmit focal depth, and the beam spacing was 298 μm. A Gaussian pulse with 5.208 MHz center frequency and 75% fractional bandwidth was used as the impulse response. The sampling frequency for the simulation was 520.8 MHz which was then decimated to 20.8 MHz.

The neural networks parameters are in Table 1. The training parameters were tuned manually and the studied image quality metrics used for evaluation purposes included contrast ratio dynamic range (CRDR) and contrast-to-noise ratio (CNR).

TABLE I. NEURAL NETWORK PARAMETERS

Parameter	Value
Architecture	Fully-connected layers
Hidden Layers	7
Layer Widths	1040
Batch Size	6000
Dropout	0.05
Batch size	6328

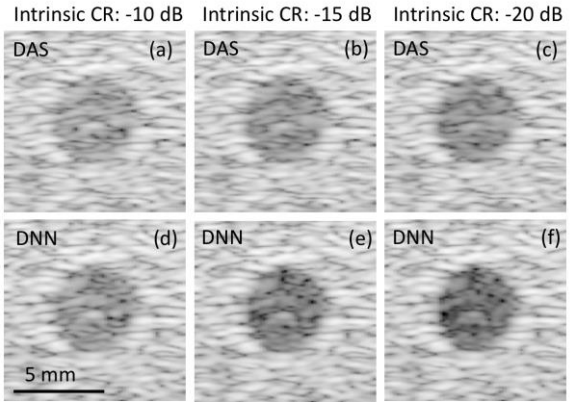

Fig. 2 (a) DAS and (b) DNN beamforming images for hypoechoic cysts with strong reverberation clutter (0 dB SCR). The images are shown with a 60 dB dynamic range.

III. RESULTS

Fig. 2 shows example images for hypoechoic cysts with varying intrinsic CR for DAS and DNN beamforming. Fig. 3 shows CR and CNR as a function of intrinsic CNR. DAS exhibited linear behavior with respect to intrinsic contrast over the range from -10 dB to 0 dB, while the DNN beamformer exhibited linear behavior from -20 dB to 0 dB. Fig. 3 shows qualitatively how the DNN beamformer improved CRDR. The difference in contrast in the DAS images for -15 dB and -20 dB CR levels shown in Figs. 2 (b) and (c) is subtle, reflecting the saturation observed for DAS at about -15 dB in Fig. 3 (a). In comparison, the difference in contrast in the DNN beamforming images for -15 dB and -20 dB CR levels shown in Figs. 2 (e) and (f) is more pronounced, demonstrating how the DNN beamformer was able to recover intrinsic contrast.

Although the speckle patterns were similar for DAS and DNN beamforming for the shown CR levels, there were observed differences, suggesting that the DNN beamformer may be starting to learn to uncover the true speckle pattern on the inside of the cyst that was masked by off-axis scattering and reverberation clutter. We note that the reverberation clutter level was high in this study, making the task of recovering the true speckle pattern on the inside of the cyst particularly challenging.

Fig. 3 (b) shows how the DNN beamformer produced the same or improved CNR for the examined values of intrinsic CR.

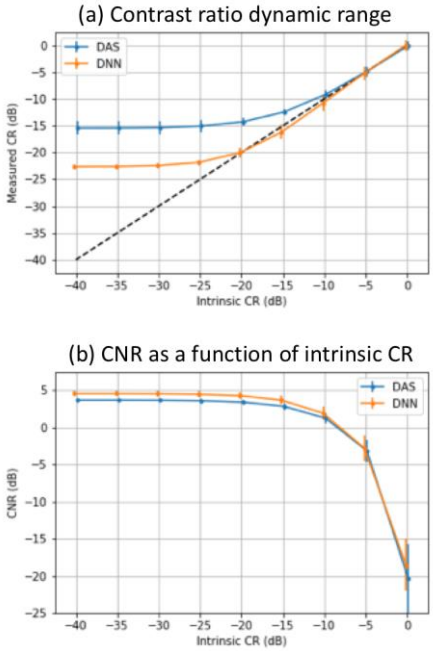

Fig. 3 (a) Contrast ratio dynamic range and (b) CNR as a function of intrinsic contrast ratio for DAS and DNN beamforming. Error bars show standard deviations for a sample size of N=3.

For a hypoechoic cyst with -20 dB intrinsic CR, the contrast-to-noise ratio (CNR) was 3.4±0.3 dB and 4.3±0.3 dB for DAS and DNN beamforming, respectively. This result demonstrates that while expanding CRDR, the DNN beamformer maintained or improved image quality as measured by CNR.

IV. CONCLUSIONS

We trained DNN beamformers to extend the CRDR of B-mode ultrasound in the presence of reverberation clutter. Overall, the results show the potential of using DNN beamformers to improve ultrasound image quality.

[1] K. Dei, A. Luchies, and B. Byram, "Contrast ratio dynamic range: A new beamformer performance metric" in Proc. of Int. Ultrason. Symp., 2017.

[2] O. M. H. Rindal, A. Rodriguez-Morales, and A. Austeng, "The dark region artifact in adaptive ultrasound beamforming," in Proc. of IEEE Ultrason. Symp., 2017.

[3] G. F. Pinton, G. E. Trahey, and J. J. Dahl, "Erratum: Sources of Image Degradation in Fundamental and Harmonic Ultrasound Imaging: A Nonlinear, Full-Wave, Simulation Study," IEEE Trans. on Ultrason., Ferroelec., Freq. Contr., vol. 58, no. 6, pp. 1272–1283, 2011.

[4] B. Byram, K. Dei, J. Tierney, and D. Dumont, "A model and regularization scheme for ultrasonic beamforming clutter reduction," IEEE Trans. on Ultrason., Ferroelec., Freq. Contr., vol. 62, no. 11, pp. 1913–1927, 2015.

[5] A. C. Luchies and B. C. Byram, "Deep Neural Networks for Ultrasound Beamforming," IEEE Trans. on Med. Imag., vol. 37, pp. 2010–2021, 2018.

[6] A. C. Luchies and B. C. Byram, "Training improvements for ultrasound beamforming with deep neural networks," Phys. in Med. And Biol., vol. 37, vol. 64, 2019.

[7] D. Hyun, L. Brickson, K. T. Looby, and J. J. Dahl, "Beamforming and Speckle Reduction Using Neural Networks," IEEE Trans. on Ultrason., Ferroelec., Freq. Contr., vol. 66, no. 5, pp. 898–910, 2019.

[8] A. Luchies and B. Byram, “High dynamic range ultrasound beamforming using deep neural networks,” in Proc. of SPIE Med. Imag., 2019.

[9] J. A. Jensen and N. B. Svendsen, "Calculation of pressure fields from arbitrarily shaped, apodized, and excited ultrasound transducers," IEEE Trans. Ultrason., Ferroelec., Freq. Contr., vol. 39, pp. 262–267, 1992.

[10] B. Byram and J. Shu, “Pseudononlinear ultrasound simulation approach for reverberation clutter,” in Journ. Med. Imag., vol. 3, no. 4, 2016.